

Fermilab-Conf-99/013-E

Tests of the Electroweak Symmetry Breaking Sector at the Tevatron ^aJ.F. DE TROCONIZ ^b*Dpto. de Física Teórica
Universidad Autónoma de Madrid,
E28049 Cantoblanco, Spain*

The phenomenology of the electroweak symmetry breaking sector is expected to involve resonances decaying preferentially into heavy fermions. Three recent CDF analyses are reviewed and used to constrain Higgs and Technicolor models.

1 Introduction

For many years the standard model has been remarkably successful at explaining and predicting experimental data. However the details of the electroweak symmetry breaking (EWSB) sector of the theory remain largely unknown, and one of the primary goals of present and future colliders is to uncover the mechanism responsible for the symmetry breaking.

In the standard model and many extensions to it, the electroweak symmetry is spontaneously broken by introducing fundamental scalar particles into the theory. These are eventually identified with W_L , Z_L , and one or more physical Higgs bosons¹. In fact the standard model incorporates the simplest implementation, with just one scalar field doublet. This leaves a single observable scalar particle, the Higgs boson, with unknown mass but fixed couplings to other particles. It should be noted that this simple model explains several striking facts, and any complication (even if possible) tends to weaken it².

Alternatively, the electroweak symmetry may be broken dynamically. This is the hallmark of technicolor (TC) theories³ in which a new strong gauge force (technicolor) and new fermions (technifermions) are introduced. The technicolor force is modelled after QCD, scaled up to the TeV scale, with the technifermions being the analogs of ordinary quarks. Technicolor acts between the technifermions to form bound states (technihadrons). In particular, the technipions include the longitudinal weak bosons, W_L and Z_L , as well as the pseudo-Goldstone bosons of dynamical symmetry breaking. Thus the dynamics

^aLecture given at the XXVth International Meeting on Fundamental Physics, La Toja, Spain, June 1998

^bRepresenting the CDF Collaboration

of the technifermions assume the role of the scalar Higgs fields in theories with spontaneous symmetry breaking.

Both models coincide in that they can be extended to generate all masses in the theory, notably the fermion masses. In the first case, explicit Yukawa couplings are used. In the second, the first TC model was augmented by Extended Technicolor (ETC)⁴. In fact, it is attractive to assume that a connection between the physics of the EWSB and the physics of flavour exists even more generally than the two previous examples. The important point is that both models now predict that the scalars (fundamental or composite) will have couplings to ordinary fermions that are proportional to mass, i.e., these scalars will decay predominantly in channels involving heavy quarks and heavy leptons. The experimental consequence of this is to provide a general frame to look for the particles involved in the EWSB, namely, to look for resonances decaying into heavy quarks and/or heavy leptons produced in pairs or in association with a W or Z .

In the following we describe three experimental searches recently published by the CDF Collaboration using $\sim 100 \text{ pb}^{-1}$ of $p\bar{p}$ collisions at the Tevatron^{5,6,7}:

- (1) Search for $X \rightarrow b\bar{b}$ in association with $W \rightarrow \ell\nu$.
- (2) Search for $X \rightarrow b\bar{b}$ in association with $V \rightarrow q\bar{q}$, where $V = W, Z$.
- (3) Search for events including a $\tau^+\tau^-$ pair and two extra jets.

No signal beyond standard model expectations has been observed in the current data sample. So in the rest of the article we will investigate the implications of this null result on the models cited at the beginning of the section, emphasizing the first-hand information on the performance of the different experimental techniques and direct evaluation of involved backgrounds. In particular we use searches (1) and (2) to constrain the production of a light standard model Higgs, and search (3) to investigate technicolor models containing a technifamily.

There are other analyses not discussed here for lack of space that can be used to find information about the EWSB sector: top physics, charged Higgs searches, etc. The reader will find information in references⁸.

2 Light Standard Model Higgs

The possible range for the mass of the standard model Higgs extends from a lower bound of about $88 \text{ GeV}/c^2$ from the LEP experiments⁹ to $\mathcal{O}(1) \text{ TeV}$. The present analysis has to be restricted to light masses for two reasons:

- The production cross sections at the Tevatron are small and decrease rapidly as a function of M_{H^0} . In $p\bar{p}$ collisions at $\sqrt{s} = 1.8$ TeV, the Higgs production mechanism with the most promising detection possibilities is $p\bar{p} \rightarrow V + H^0$, with $V = W, Z$. In the framework of the standard model, the production cross section in this channel is 1.3 to 0.11 pb for Higgs masses between 70 to 140 GeV/ c^2 ¹⁰.
- The technique used is to look for resonances in the $b\bar{b}$ channel. $H^0 \rightarrow b\bar{b}$ is the dominant decay mode of the Higgs boson only up to $M_{H^0} \sim 130$ GeV/ c^2 .

However there are two important motivations to emphasize the region of light Higgs masses:

- Precision electroweak experiments suggest that the Higgs boson mass may lie at the lower end of the open range¹¹.
- A similar symmetry breaking mechanism occurs in the minimal supersymmetric extension of the standard model, where several observable scalar states are predicted, the lightest of which is expected to decay predominantly into $b\bar{b}$ states and to have a mass below 135 GeV/ c^2 ¹².

The cross sections expected in the standard model are out of the scope of the present analysis, using ~ 100 pb⁻¹ of $p\bar{p}$ collisions. We therefore report on a general search for a Higgs scalar produced in association with a vector boson with unknown cross section σ_{VH^0} . We look for H^0 decays to a $b\bar{b}$ pair with unknown branching ratio β , and for two possible decays of the vector boson: (i) $W \rightarrow \ell\nu$ with $\ell = e, \mu$ and (ii) $V \rightarrow q\bar{q}$. Finally, the limits obtained in both channels are combined.

2.1 Leptonic Analysis

The experimental signature considered is WH^0 with $W \rightarrow e\nu$ or $\mu\nu$, and $H^0 \rightarrow b\bar{b}$, giving final states with one high- p_T lepton, large missing transverse energy (\cancel{E}_T) due to the undetected neutrino, and two b jets⁵. The ability to tag b jets with high efficiency and a low mistag rate is vital for searching for the decay of $H^0 \rightarrow b\bar{b}$. We use the secondary vertex (SECVTX) and soft-lepton (SLT) b -tagging algorithms developed for the top quark discovery¹³.

A three-level trigger selects events that contain an electron or muon for this analysis. The event selection starts with the requirement of a primary lepton, either an isolated electron with $E_T > 20$ GeV¹⁴ or an isolated muon with $p_T > 20$ GeV/ c , in the central region $|\eta| < 1.0$. A W boson sample

Table 1: The expected number of tagged $W + n$ jet events from QCD backgrounds and top production compared the observed number of events.

	$W + 1$ jet	$W + 2$ jet	$W + 3$ jet	$W + \geq 4$ jet
Events with single tag				
Expected	67 ± 13	30 ± 5	16 ± 2	13 ± 3
Observed	66	36	11	12
Events with double tag				
Expected	0	3.0 ± 0.6	3.6 ± 0.6	5.2 ± 1.1
Observed	0	6	6	2

is selected by requiring $\cancel{E}_T > 20$ GeV. Events which contain a second, same flavour lepton with $p_T > 10$ GeV/ c are removed as possible Z boson candidates if the reconstructed ee or $\mu\mu$ invariant mass is between 75 and 105 GeV/ c^2 . The events must also not be accepted by the CDF top dilepton analysis¹³. To further reduce the dilepton backgrounds, we reject events with an additional high- p_T isolated track with opposite charge to that of the primary lepton. The remaining events are classified according to jet multiplicity. Jets are defined as localized energy depositions in the calorimeters and are reconstructed using an iterative clustering algorithm with a fixed cone of radius $\Delta R = \sqrt{\Delta\eta^2 + \Delta\phi^2} = 0.4$ in $\eta - \phi$ space¹⁵. Jet energies are then corrected for energy losses in uninstrumented detector regions, energy falling outside the clustering cone, contributions from underlying event and multiple interactions, and calorimeter nonlinearities.

The $W + 2$ jet bin is expected to contain most of the signal, while the other bins are used to check the background calculation. In order to enhance the signal in the $W + 2$ jet bin, we require that one or both of the jets be identified ('tagged') as coming from a b hadron. We require at least one jet to be tagged by the SECVTX algorithm, which has a higher signal-to-noise ratio than the SLT algorithm. For the single-tag analysis, the other jet must not be tagged, while for the double-tag analysis the second jet must be tagged by either SECVTX or SLT.

The SECVTX tagging algorithm begins by searching for secondary vertices that contain three or more displaced tracks. If none are found, the algorithm searches for two-track vertices using more stringent track criteria. A jet is tagged if the secondary vertex transverse displacement from the primary one exceeds three times its uncertainty.

The SLT tagging algorithm identifies electrons and muon from semileptonic b decays by matching tracks with $p_T > 2$ GeV/ c with clusters of electromagnetic energy in the calorimeters or tracks in the muon chambers. To

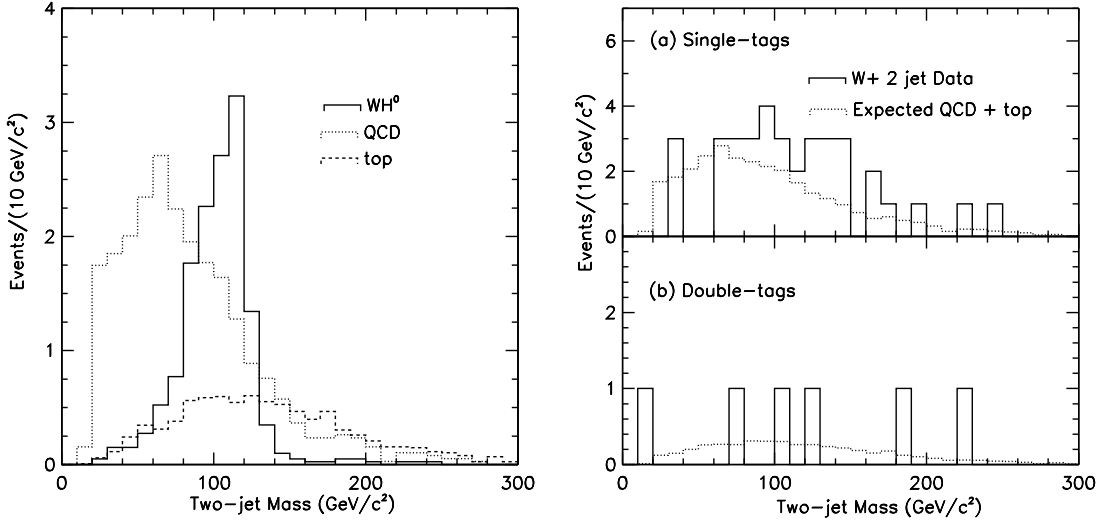


Figure 1: (Left) The expected tagged two-jet mass distribution from QCD (dotted), top (dashed), and WH^0 production (solid) with $M_{H^0} = 110 \text{ GeV}/c^2$. The WH^0 distribution has been scaled up by a factor of 50. (Right) The measured two-jet mass distribution in the data along with background expectations from (a) single-tagged events and (b) double-tagged events.

gain additional background rejection, we require the track to lie within a cone $\Delta R < 0.4$ of the axis of a jet and to be displaced in the transverse plane from the primary vertex by at least two standard deviations in the jet direction. This latter requirement reduces lepton misidentifications by a factor of five while retaining 65% of the efficiency.

The total acceptance is calculated as a product of the kinematic and geometric acceptance, trigger, lepton identification, and b -tagging efficiencies, and the W leptonic branching ratios. The acceptance for identifying WH^0 is calculated from data and a standard model simulation of Higgs production, where the Higgs is forced to decay into $b\bar{b}$ with 100% branching ratio. The acceptance increases monotonically from $0.53 \pm 0.13\%$ ($0.17 \pm 0.04\%$) to $1.1 \pm 0.3\%$ ($0.42 \pm 0.11\%$) for single (double) tagging as M_{H^0} increases from 70 to 120 GeV/c^2 . A 25% systematic in the acceptance comes from uncertainties in the modeling of initial and final state radiation, jet energy, and b -tag, trigger, and lepton identification efficiencies.

Background events come predominantly from the direct production of W

bosons in association with heavy quarks (estimated using the HERWIG Monte Carlo program), mistags (from generic jet data), and $t\bar{t}$ production (normalized to the CDF measured cross section $\sigma_{t\bar{t}} = 7.6^{+1.8}_{-1.5}$ pb¹⁶). Other small backgrounds are estimated from a combination of Monte Carlo simulations and data.

The numbers of observed single-tagged and double-tagged events and the corresponding background estimates are shown in Table 1. By construction, data and expectations are in reasonably good agreement in the $W + \geq 3$ jet bins, which, along with other $t\bar{t}$ decay channels, were used to measure the $t\bar{t}$ production cross section. The number of b -tags in the $W + 2$ jet bin can be compared to the background calculation. This bin shows a small excess of events corresponding to one standard deviation.

To increase the sensitivity of the search we look for a resonant mass peak in the reconstructed two-jet invariant mass distribution using the 4-momenta of the jets as measured by the calorimeter. The expected two-jet invariant mass shape for WH^0 production is shown in Figure 1 (left) for $M_{H^0} = 110$ GeV/ c^2 . The distributions for the data are shown in Figure 1 (right), along with the background expectation.

We set an upper limit on the production cross section times branching ratio of $p\bar{p} \rightarrow WH^0$ as a function of M_{H^0} , by fitting the number of events in the $W + 2$ jet samples and the shape of the two-jet mass distributions. The fit yields $\sigma_{WH^0} \cdot \mathcal{B}(H^0 \rightarrow b\bar{b})$ in the range from $0.2^{+4.7}_{-0.0}$ to $5.7^{+4.2}_{-3.0}$ pb for a new particle of mass between 70 and 120 GeV/ c^2 , statistically compatible with no signal. From the 95% C.L. limits on $\sigma(p\bar{p} \rightarrow WH^0)$, the corresponding limits on VH^0 production were calculated. We used the program PYTHIA to compute the standard model prediction for the ratio $\sigma(ZH^0)/\sigma(WH^0)$. The leptonic analysis efficiency for ZH^0 events relative to that for WH^0 events was estimated to be $(10 \pm 2)\%$. The limits are summarized in Table 2.

2.2 Hadronic Analysis

The experimental signature considered is four jets in the final state, with two of them identified as b jets⁶. The hadronic channel described here has the advantage of a larger branching ratio, and is sensitive to both WH^0 and ZH^0 production ($\sigma(ZH^0)/\sigma(WH^0) \sim 0.6$), but suffers from a larger QCD background.

The data sample was recorded with a trigger which requires four or more clusters of contiguous calorimeter towers, each with transverse energy $E_T \geq 15$ GeV, and a total transverse energy $\sum E_T \geq 125$ GeV. Offline, events are required to have four or more jets with uncorrected $E_T > 15$ GeV and $|\eta| < 2.1$.

Table 2: Summary of the hadronic analysis fit results, standard model predictions for $\beta\sigma$, and 95% C.L. limits from the hadronic, leptonic, and combined analyses.

M_{H^0} (GeV/ c^2)	$\beta\sigma$ (pb) fit	$\beta\sigma$ (pb) SM	$\beta\sigma$ (pb) had. limit	$\beta\sigma$ (pb) lep. limit	$\beta\sigma$ (pb) comb. limit
70	44 ± 42	1.13	117.3	21.9	23.1
80	0_{-0}^{+19}	0.76	53.2	28.2	23.8
90	$0.0_{-0.0}^{+9.7}$	0.55	28.9	29.0	18.0
100	$0.0_{-0.0}^{+7.6}$	0.41	22.8	27.2	16.8
110	$0.0_{-0.0}^{+6.3}$	0.30	18.7	30.1	17.1
120	$0.0_{-0.0}^{+5.9}$	0.20	17.6	25.0	16.0
130	$0.0_{-0.0}^{+5.5}$	0.12	16.7	38.5	19.7
140	$0.0_{-0.0}^{+5.1}$	0.06	15.3	34.5	17.2

After this initial selection the sample contains 207,604 events. In addition, we require that at least two among the four highest- E_T jets in the event tagged by the SECVTX algorithm.

There are 764 events with four or more jets and two or more b -tags. In these events, only the four highest- E_T jets are considered for the mass reconstruction: the two highest- E_T b -tagged jets are assigned to the Higgs boson, and the other two to the vector boson. The $b\bar{b}$ invariant mass distribution in signal events contains a Gaussian core with a sigma of $\sim 0.14 \times M_{H^0}$. The tails of the distribution are dominated by the cases (25-30%) where the jet assignment in the mass reconstruction is incorrect. In most of these cases, one of the jets assigned to the Higgs is a heavy quark jet from the decay of the V boson.

The challenge of this analysis is to understand the sample composition. The main source of background events is QCD heavy flavor production. The heavy flavor content of QCD hard processes has been modelled with PYTHIA. We generated all QCD jet production channels and retained the events that contained a heavy quark produced either in the hard scattering or in the associated radiation process. Events with a heavy quark are conventionally classified in three groups: direct production, gluon splitting, and flavor excitation. Direct production events are characterized by a high value of the invariant mass, $M_{b\bar{b}}$, and a low value of the transverse momentum of the $b\bar{b}$ system, $p_T(b\bar{b})$. The same is true for flavor excitation events. The kinematics of final state gluon splitting events favor a relatively smaller invariant mass value and a large $p_T(b\bar{b})$, since both jets tend to be emitted along the same direction. In this plane, the Higgs signal shows a greater tendency to large $M_{b\bar{b}}$ and $p_T(b\bar{b})$.

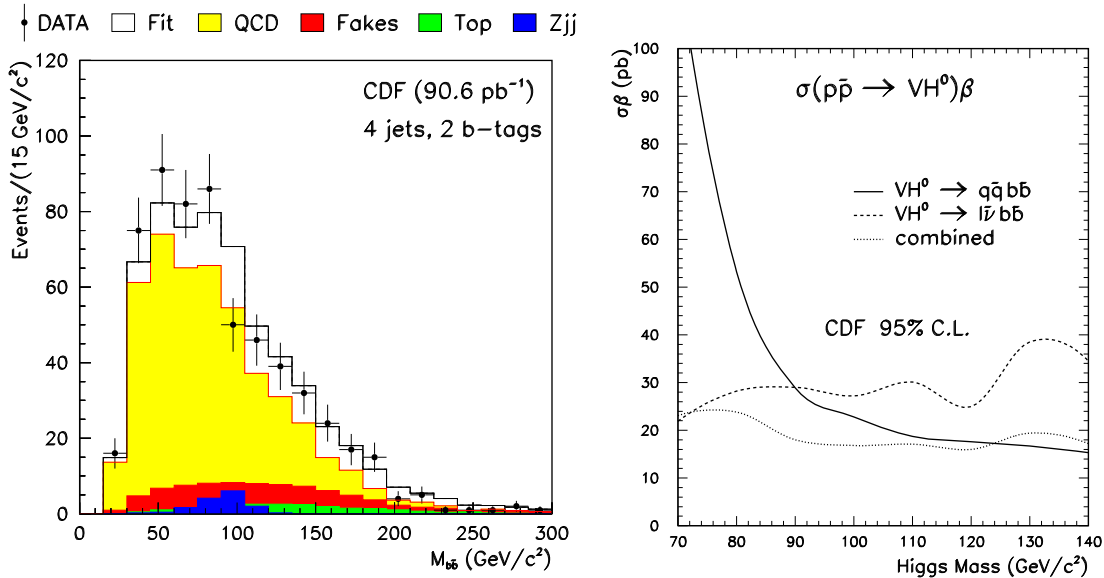


Figure 2: (Left) The measured invariant mass distribution from double-tagged events (points) compared to the fit prediction. The solid line is the sum of the QCD, fakes, $t\bar{t}$, and Z + jets components. (Right) The CDF 95% C.L. upper limits on $\sigma(pp \rightarrow VH^0) \cdot \beta$ where $\beta = \mathcal{B}(H^0 \rightarrow b\bar{b})$.

values. A cut on $p_T(b\bar{b}) \geq 50$ GeV/ c is $\sim 80\%$ efficient for the signal and strongly discriminates against direct production and flavor excitation of heavy quarks. After the $p_T(b\bar{b})$ requirement is applied to the data 589 events remain.

Other backgrounds are $t\bar{t}$ production, Z + jets events with $Z \rightarrow b\bar{b}/c\bar{c}$ and fake double-tags. The first two are estimated from Monte Carlo and the last one from data. Using the CDF measured $t\bar{t}$ production cross section and a top quark mass of $M_t = 175$ GeV/ c^2 , HERWIG predicts 26 ± 7 $t\bar{t}$ events in the data, after trigger, kinematic and b -tag requirements. The same generator predicts 17 ± 4 Z + jets background events. Fake double-tags are defined as events in which at least one of the two tagged jets contains a false secondary vertex in a light quark or gluon jet. Fake tag probabilities are parameterized by measuring in several inclusive jet data samples the proportion of jets in which a secondary vertex is reconstructed on the wrong side of the primary vertex with respect to the jet direction¹³. The current data set is estimated to contain 89 ± 11 fake double-tag events. Finally, other minor sources of

background account for less than 1% of the total number of events, have a broad invariant mass distribution, and are neglected in the final fit.

The total signal detection efficiency is defined as the product of the trigger efficiency, the kinematical and geometrical acceptances, the double b -tagging efficiency, the $p_T(b\bar{b})$ cut efficiency, and the V hadronic branching fractions. The total efficiency increases linearly from $0.6 \pm 0.1\%$ to $2.2 \pm 0.6\%$ for Higgs masses ranging from $70 \text{ GeV}/c^2$ to $140 \text{ GeV}/c^2$.

The shape of the observed b -tagged dijet invariant mass distribution is fit, using a binned maximum-likelihood method, to a combination of signal, fake double-tag events, and QCD, $t\bar{t}$ and $Z + \text{jets}$ backgrounds. The QCD and signal normalizations are left free in the fit while the normalizations of the $t\bar{t}$, $Z + \text{jets}$ and fakes are constrained by Gaussian functions to their expected values and uncertainties.

The fit yields $\sigma_{VH^0} \cdot \beta = 44 \pm 42 \text{ pb}$ for $M_{H^0} = 70 \text{ GeV}/c^2$, statistically compatible with zero signal. For larger masses, zero signal contribution is preferred. Table 2 shows the result of the fits as a function of the Higgs mass. Figure 2 (left) shows the b -tagged dijet invariant mass distribution for the data compared to the results of the fit for $M_{H^0} \geq 80 \text{ GeV}/c^2$.

Since the observed distribution is consistent with standard model background expectations, we place limits on $p\bar{p} \rightarrow VH^0$ production. Systematic uncertainties on the 95% C.L. limits arise from luminosity, jet energy scale, double b -tagging efficiencies, QCD radiation, limited Monte Carlo statistics, and background normalizations and shapes. The total systematic uncertainty is in the range 26%–30%. The 95% C.L. limits are summarized in Table 2 and Figure 2 (right). The resulting bounds fall rapidly from 117 pb at $M_{H^0} = 70 \text{ GeV}/c^2$ to values between 15 and 20 pb for $M_{H^0} > 105 \text{ GeV}/c^2$.

2.3 Combined results

To combine the two results presented above, the data from both channels were then fitted simultaneously⁶. Correlations between systematic uncertainties due to luminosity, QCD radiation, and b -tagging efficiency were taken into account. All other systematic uncertainties were considered uncorrelated. The 95% C.L. limits range from 16 to 24 pb and are shown in Table 2 and Figure 2 (right).

3 Technicolor

Now we turn to the second mechanism of EWSB discussed in the Introduction⁷. Particularly interesting from the present experimental point of view^{17,18} are TC models containing a technifamily, i.e. a set of technifermions with the same

Table 3: The 95% confidence level upper limits on the leptoquark (color-triplet technipion) production cross section times branching ratio squared as a function of $M(\pi_{LQ})$ and $M(\rho_T)$, for $\Delta M = 50 \text{ GeV}/c^2$. Numbers are given in pb.

$M(\pi_{LQ})$ (GeV/ c^2)	$M(\rho_T)$ (GeV/ c^2)										
	200	250	300	350	400	450	500	550	600	650	700
100	12.7	9.8	8.2	7.4	7.2	7.7	8.5	9.4	9.8	10.0	10.2
125		6.4	5.3	4.6	4.1	3.9	3.9	4.1	4.5	4.8	5.0
150			4.7	4.1	3.6	3.3	3.1	3.0	3.1	3.2	3.5
175				3.7	3.3	3.1	2.9	2.7	2.6	2.6	2.7
200					3.4	3.0	2.8	2.5	2.3	2.2	2.1
225						2.9	2.7	2.5	2.3	2.2	2.1
250							2.8	2.5	2.3	2.2	2.1
275								2.5	2.3	2.2	2.0
300									2.3	2.2	2.0

structure and quantum numbers of a complete standard model generation of quarks and leptons, and carrying an additional TC quantum number. By convention, technifermions which are color-triplets of ordinary QCD are called techniquarks, and color-singlet technifermions are called technileptons. The particle spectrum of these models includes color-singlet, -triplet and -octet technipions. The technipions (π_T) decay via ETC interactions. Since these are also responsible for the fermion masses, technipions are expected to have Higgs-boson-like couplings to ordinary fermions, i.e. to decay preferentially to third-generation quarks and leptons. In particular, the color-triplet technipions are an example of scalar third-generation leptoquarks (π_{LQ}). In this section, we use the results of a search for third-generation leptoquarks by CDF, in order to explore TC models containing a technifamily. Other experimental constraints on these models come from precision electroweak measurements at LEP^{19,20}, and from measurements of the $b \rightarrow s\gamma$ decay rate²¹.

Let's consider technicolor models containing a family of color-singlet technileptons and color-triplet techniquarks. In these models, there is a color-octet vector resonance, called technirho (ρ_T), with the quantum numbers of the gluon. Leptoquarks are assumed to be pair produced via gluon-gluon fusion and $q\bar{q}$ annihilation. In $q\bar{q}$ and gg collisions, the ρ_T couples to the gluon propagator enhancing s-channel reactions (Fig. 3), analogously to the vector-meson-dominance description of the process $e^+e^- \rightarrow \pi^+\pi^-$ ²². Two decay modes may exist for the technirho¹⁸: $\rho_T \rightarrow q\bar{q}, gg$ and $\rho_T \rightarrow \pi_T\bar{\pi}_T$. If the ρ_T mass is less than twice the π_T mass, only the $q\bar{q}, gg$ decay mode is possible, resulting in resonant dijet production. A search result for the dijet signal of

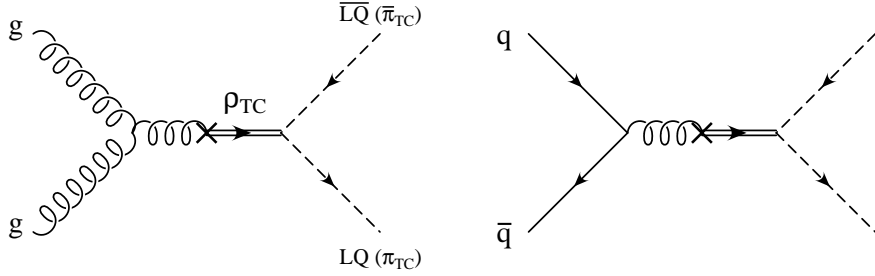


Figure 3: The resonant production of technipion pairs. The technirho couples directly to the gluon via vector-meson-dominance enhancing s-channel production.

ρ_T has already been reported by CDF. The CDF-measured dijet mass spectrum excludes ρ_T with masses in the range $260 < M(\rho_T) < 480 \text{ GeV}/c^2$ at the 95% C.L.²³. If the ρ_T mass is larger than twice the π_T mass, the ρ_T decays preferentially into π_T pairs.

The technipion spectrum of the technifamily model was estimated in^{24,18}. It contains color-singlet, -triplet and -octet (π_8) technipions. The octets are heavier than the triplets, and these are heavier than the singlets. We make the simplifying assumption that there is no mass splitting among the different octet and triplet technipions. We consider the class of color-triplet technipions decaying via $\pi_{LQ} \rightarrow \bar{b}\tau^-$ ($\bar{\pi}_{LQ} \rightarrow b\tau^+$) with branching fraction β .

The leading-order leptoquark pair production cross section depends only on the technirho mass ($M(\rho_T)$), the leptoquark mass ($M(\pi_{LQ})$), and the technirho width ($\Gamma(\rho_T)$). $M(\pi_{LQ})$ and $M(\rho_T)$ are treated as independent free parameters. $\Gamma(\rho_T)$ can be calculated as a function of four more basic quantities, $\Gamma(\rho_T) = \Gamma(M(\rho_T), M(\pi_{LQ}), \Delta M, N_{TC})$, where $\Delta M = M(\pi_8) - M(\pi_{LQ})$, and N_{TC} is the number of technicolors. We consider $M(\rho_T)$, $M(\pi_{LQ})$, ΔM , and N_{TC} as the four continuous parameters of the theory. We set limits in the $M(\pi_{LQ}) - M(\rho_T)$ plane. We probe the dependence of the production cross section on $\Gamma(\rho_T)$ by fixing $N_{TC} = 4$, while allowing ΔM to take one expected and two limiting values. ETC and QCD corrections to $M(\pi_8)$ and $M(\pi_{LQ})$ are responsible for ΔM , analogously to the QED corrections to $M(\pi^0)$ and $M(\pi^\pm)$. ΔM is expected to be around $50 \text{ GeV}/c^2$ ¹⁸. We take $\Delta M = 0$ and $\Delta M = \infty$ as two extreme values. The resulting variation in $\Gamma(\rho_T)$ could also have been obtained changing N_{TC} by a factor of 4, for a fixed $\Delta M = 50 \text{ GeV}/c^2$.

The experimental signature considered is $\tau^+\tau^-$ plus two jets in the final state, in the case where one τ decays leptonically and the other decays hadron-

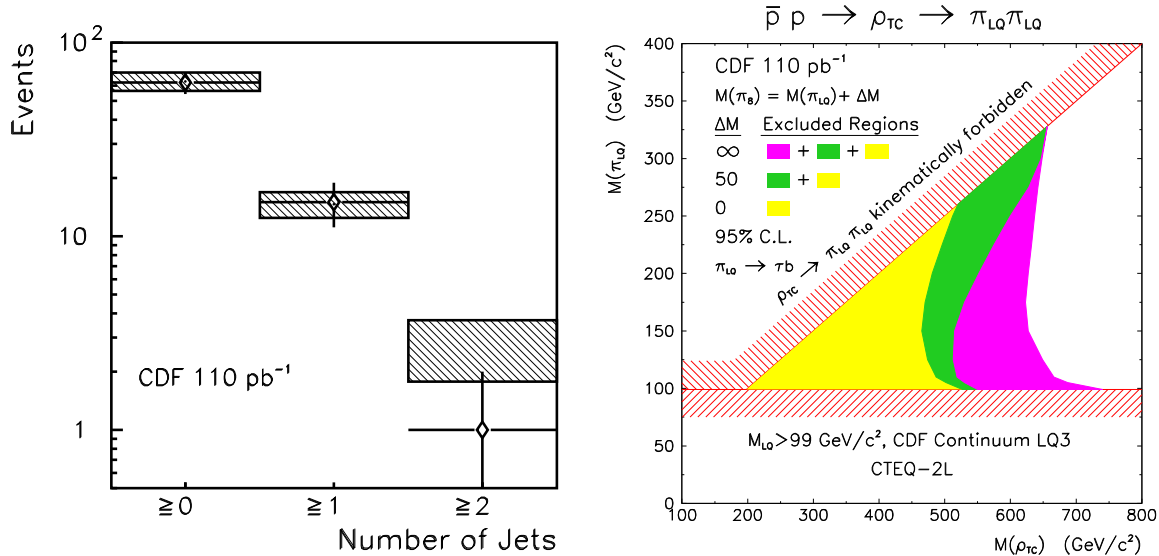


Figure 4: (Left) The inclusive jet multiplicity in $\tau^+\tau^-$ candidate events (diamonds) compared to standard model expectations. (Right) The 95% C.L. exclusion regions in the $M(\pi_{LQ}) - M(\rho_T)$ plane. The three shaded areas correspond (from left to right) to technipion mass splitting values of 0, 50 GeV/c² and ∞ , respectively.

ically. The analysis selects a 110 pb⁻¹ data set containing an isolated electron or muon in the region $|\eta| < 1$ with $p_T > 20$ GeV/c¹⁴, and an isolated, highly-collimated hadronic jet consistent with a hadronic tau decay. Hadronic τ candidates (τ -jets) are selected from jets that have an uncorrected total transverse energy of $E_T > 15$ GeV in the region $|\eta| < 1$. The associated charged particles with $p_T > 1$ GeV/c in a 10^o cone around the jet direction must satisfy the following requirements: (i) the τ -jet must have one or three charged particles; (ii) if there are three, the scalar sum p_T must exceed 20 GeV/c and the invariant mass must be smaller than 2 GeV/c²; and (iii) the leading charged particle must have $p_T > 10$ GeV/c and must point to an instrumented region of the calorimeter. The efficiency of the τ -jet identification criteria grows from 32% for τ -jets in the range $15 < E_T < 20$ GeV to a plateau value of 59% for $E_T > 40$ GeV. Isolated τ -jets must have no charged particles with $p_T > 1$ GeV/c in the annulus between 10^o and 30^o around the jet axis. Events where the high- p_T lepton is consistent with originating from a $Z \rightarrow ee$ or $Z \rightarrow \mu\mu$

decay are removed. In addition, the analysis uses the missing transverse energy characteristic of neutrinos from tau decays. The requirement $\Delta\Phi < 50^\circ$, where $\Delta\Phi$ is the azimuthal separation between the directions of the missing transverse energy \cancel{E}_T and the lepton, distinguishes $\tau^+\tau^-$ events from backgrounds such as $W + \text{jets}$. Figure 4 (left) shows the jet multiplicity in $\tau^+\tau^-$ candidate events. The agreement with the standard model background prediction is excellent. Finally, two or more jets with $E_T > 10$ GeV and $|\eta| < 4.2$, assumed to originate from b quark hadronization, are required. One leptoquark pair candidate event survives these selection criteria. The observed yield is consistent with the $2.4^{+1.2}_{-0.6}$ expected background events from standard model processes, dominated by $Z \rightarrow \tau\tau + \text{jets}$ production (2.1 ± 0.6) with the remainder from diboson and $t\bar{t}$ production⁷.

The detection efficiencies for the signal are determined using a full leading-order matrix element calculation for technipion pair production (continuum, resonant, and interference terms are included)¹⁸ and embedded in the PYTHIA Monte Carlo program to model the full $p\bar{p}$ event structure. The generated events are passed through a detector simulation program and subjected to the same search requirements as the data. The total efficiency increases from 0.3% for $M(\rho_T) = 200$ GeV/ c^2 and $M(\pi_{LQ}) = 100$ GeV/ c^2 , to 1.8% for $M(\rho_T) = 700$ GeV/ c^2 and $M(\pi_{LQ}) = 300$ GeV/ c^2 . The systematic errors in the efficiencies were estimated as described in⁷, including uncertainties in the modelling of gluon radiation, in the calorimeter energy scale, in the dependence on renormalization scales, and in the luminosity measurement. They range from 15% for $M(\rho_T) = 200$ GeV/ c^2 and $M(\pi_{LQ}) = 100$ GeV/ c^2 , to 10% for $M(\pi_{LQ}) \geq 125$ GeV/ c^2 .

We place limits on the leptoquark pair production cross section times branching ratio squared within the framework of the technicolor model described above. Table 3 lists the leptoquark 95% confidence level upper limits on the production cross section times branching ratio squared as a function of $M(\pi_{LQ})$ and $M(\rho_T)$, for $\Delta M = 50$ GeV/ c^2 . These numbers differ by at most 1 pb from the corresponding limits for $\Delta M = 0$ and $\Delta M = \infty$ when $M(\pi_{LQ}) < 175$ GeV/ c^2 . For larger values of $M(\pi_{LQ})$ the differences are negligible. Comparing to the theoretical expectations for $\sigma(p\bar{p} \rightarrow \pi_{LQ}\bar{\pi}_{LQ}) \cdot \beta^2$, we place bounds in the $M(\pi_{LQ}) - M(\rho_T)$ plane. Figure 4 (right) shows the 95% C.L. mass exclusion regions. The upper part of the plot corresponds to the kinematically forbidden region where $M(\rho_T) < 2M(\pi_{LQ})$. The bottom region is the exclusion area from the continuum leptoquark analysis, $M(\pi_{LQ}) \geq 99$ GeV/ c^2 ⁷. The three shaded areas from left to right correspond to technipion mass splitting values of $\Delta M = 0, 50$ GeV/ c^2 and ∞ , respectively. Although more information is presented in Figure 4, it is useful to summarize our tech-

nirho excluded region using a single number. For $\Delta M = 0$ (50, ∞) and $M(\pi_{LQ}) < M(\rho_T)/2$, we exclude color octet technirhos with mass less than 465 (513, 622) GeV/c^2 at 95% confidence level.

4 Discussion and Prospects

We have described several attempts to explore the phenomenology of the EWSB sector at the Tevatron. A first kind of analyses tried to reconstruct $b\bar{b}$ resonances. From the experimental point of view, this involved the study and development of a number of techniques of broad interest for the hadron collider experiments of the next decade. These include jet spectroscopy, b -tagging algorithms, and quantitative evaluation of challenging new backgrounds as QCD production of heavy quarks in a multijet environment.

No signal has been found yet, and the results have been used to constrain the production of a light standard model Higgs. The Higgs searches have not provided yet any lower Higgs mass bound. The sensitivity of the present search is limited by statistics to a cross section approximately two orders of magnitude larger than the predicted cross section for standard model Higgs production¹⁰. It also should be noted that, because these limits were derived from a shape fit, they only apply to a very restricted region of parameter space in the minimal supersymmetric extension of the standard model.

For the next Tevatron run CDF hopes for an approximately twenty-fold increase in the total integrated luminosity and a factor of two improvement in the double b -tagging efficiency. D0 will be as good as CDF in this respect. However, this is still insufficient to reach say a 120 GeV/c^2 Higgs mass, unless the total detection efficiency be improved by one order of magnitude. The viability of this improvement is at present under study²⁵. Plans include the installation of dedicated Higgs triggers, systematic inclusion of all relevant channels (notably ZH^0 production, with $Z \rightarrow \ell\ell$ and $Z \rightarrow \nu\nu$), finer mass resolution, and additional, more efficient selection algorithms (e.g., neural networks).

Another analysis described a virtually background-free search of resonances decaying into τ leptons. The four objects appearing in the selected events can be arranged in two ways. Looking for τ -jet leptoquark resonances the analysis can be used to directly constrain TC models including one technifamily. The expected factor $\times 20$ in luminosity will help to push the technirho mass limits closer to the TeV region. Interpreted as containing a $\tau^+\tau^-$ resonance, the same events can be used to test effectively the large $\tan(\beta)$ region of the SUSY extension of the standard model²⁶.

In conclusion, we are just at the very beginning of this kind of physics at hadron colliders. Most importantly we need data to look at, and for that

reason the CDF and D0 Collaborations are looking forward to Run 2 with great anticipation.

Acknowledgments

I would like to thank Prof. B. Adeva and collaborators for the stimulating atmosphere of the meeting and warm hospitality.

References

1. P.W. Higgs, Phys. Lett. **12**, 132 (1964), Phys. Rev. Lett. **13**, 508 (1964), Phys. Rev. **145**, 1156 (1966); F. Englert and R. Brout, Phys. Rev. Lett. **13**, 321 (1964).
2. M. Veltman, Report No. CERN-97-05.
3. S. Weinberg, Phys. Rev. D **19**, 1277 (1979); L. Susskind, Phys. Rev. D **20**, 2619 (1979).
4. S. Dimopoulos and L. Susskind, Nucl. Phys. **B155**, 237, (1979); E. Eichten and K. Lane, Phys. Lett. B **90**, 125 (1980).
5. F. Abe *et al.*, Phys. Rev. Lett. **79**, 3819 (1997).
6. F. Abe *et al.*, Phys. Rev. Lett. **81**, 5748 (1998).
7. F. Abe *et al.*, Phys. Rev. Lett. **78**, 2906 (1997); Report No. Fermilab-Pub-98-352-E.
8. S. Abachi *et al.*. Report No. Fermilab-Conf-96-258-E, 1996; F. Abe *et al.*, Phys. Rev. Lett. **79**, 357 (1997); B. Bevensee, Report No. Fermilab-Conf-98-155-E, 1998; K. Tollefson, Report No. Fermilab-Conf-98-389-E, 1998.
9. M. Acciarri *et al.*, Phys. Lett. **B 431** 437 (1998); R. Barate *et al.*, Phys. Lett. **B 440** 403 (1998); G. Abbiendi *et al.*, Report No. CERN-EP-98-173.
10. S.L. Glashow, D.V. Nanopoulos and A. Yildiz, Phys. Rev. D **18**, 1724 (1978); A. Stange, W. Marciano and S. Willenbrock, Phys. Rev. D **49**, 1354 (1994); Phys. Rev. D **50**, 4491 (1994).
11. F. Teubert, Invited Talk at the IVth International Symposium on Radiative Corrections, Barcelona, 1998.
12. M. Carena *et al.*, Nucl. Phys. **B 461** 407 (1996); H. E. Haber *et al.*, Z. Phys. **C75** 539 (1997).
13. F. Abe *et al.*, Phys. Rev. Lett. **74**, 2626 (1995).
14. In the CDF coordinate system, ϕ and θ are the azimuthal and polar angles with respect to the proton beam direction. The pseudorapidity η is defined as $-\ln[\tan(\theta/2)]$. The transverse momentum of a particle is $p_T = p \sin \theta$. The analogous quantity using calorimeter energies is called

the transverse energy E_T . The difference between the vector sum of all the transverse energies and zero is the missing transverse energy \cancel{E}_T .

15. F. Abe *et al.*, Phys. Rev. D **45**, 1448 (1992).
16. F. Abe *et al.*, Phys. Rev. Lett. **80**, 2773 (1998).
17. E. Eichten, I. Hinchliffe, K. Lane, and C. Quigg, Rev. Mod. Phys. **56**, 579 (1984); Phys. Rev. D **34**, 1547 (1986).
18. K. Lane and M.V. Ramana, Phys. Rev. D **44**, 2678 (1991).
19. M. Martinez *et al.*, Report No. CERN-EP-98-27, 1998, submitted to Rep. Mod. Phys..
20. R.S. Chivukula, S. B. Selipsky, and E.H. Simmons, Phys. Rev. Lett. **69**, 575 (1992); R.S. Chivukula, E.H. Simmons, and J. Terning, Phys. Lett. B **331**, 383 (1994).
21. B. Balaji, Phys. Rev. D **53**, 1699 (1996); C. Lu and Z. Xaio, Phys. Rev. D **53**, 2529 (1996).
22. J.J. Sakurai, *Currents and Mesons* (Chicago University Press, Chicago, IL, 1969).
23. F. Abe *et al.*, Phys. Rev. D **55**, 5263 (1997); Report No. Fermilab-Pub-98-290-E.
24. M.E. Peskin, Nucl. Phys. **B175**, 197 (1980); J. Preskill, Nucl. Phys. **B177**, 21 (1981).
25. J. Conway, Talk at the Tevatron Run 2 SUSY/Higgs Workshop, Fermilab, 1998.
26. M. Drees *et al.*, Phys. Rev. Lett. **80**, 2047 (1998); Erratum *ibid.* **81**, 2394 (1998).